CrossMark

Erosion Performance of Gadolinium Zirconate-Based Thermal Barrier Coatings Processed by Suspension Plasma Spray

Satyapal Mahade[1] · Nicholas Curry[2] · Stefan Björklund[1] · Nicolaie Markocsan[1] ·
Per Nylén[1] · Robert Vaßen[3]

Abstract 7-8 wt.% Yttria-stabilized zirconia (YSZ) is the standard thermal barrier coating (TBC) material used by the gas turbines industry due to its excellent thermal and thermo-mechanical properties up to 1200 °C. The need for improvement in gas turbine efficiency has led to an increase in the turbine inlet gas temperature. However, above 1200 °C, YSZ has issues such as poor sintering resistance, poor phase stability and susceptibility to calcium magnesium alumino silicates (CMAS) degradation. Gadolinium zirconate (GZ) is considered as one of the promising top coat candidates for TBC applications at high temperatures (>1200 °C) due to its low thermal conductivity, good sintering resistance and CMAS attack resistance. Single-layer 8YSZ, double-layer GZ/YSZ and triple-layer GZdense/GZ/YSZ TBCs were deposited by suspension plasma spray (SPS) process. Microstructural analysis was carried out by scanning electron microscopy (SEM). A columnar microstructure was observed in the single-, double- and triple-layer TBCs. Phase analysis of the as-sprayed TBCs was carried out using XRD (x-ray diffraction) where a tetragonal prime phase of zirconia in the

single-layer YSZ TBC and a cubic defect fluorite phase of GZ in the double and triple-layer TBCs was observed. Porosity measurements of the as-sprayed TBCs were made by water intrusion method and image analysis method. The as-sprayed GZ-based multi-layered TBCs were subjected to erosion test at room temperature, and their erosion resistance was compared with single-layer 8YSZ. It was shown that the erosion resistance of 8YSZ single-layer TBC was higher than GZ-based multi-layered TBCs. Among the multi-layered TBCs, triple-layer TBC was slightly better than double layer in terms of erosion resistance. The eroded TBCs were cold-mounted and analyzed by SEM.

Keywords columnar microstructure · erosion test · gadolinium zirconate · multi-layered thermal barrier coating · suspension plasma spray · yttria-stabilized zirconia

✉ Satyapal Mahade
satyapal.mahade@hv.se

1 Department of Engineering Science, University West, Trollhättan, Sweden

2 Treibacher Industrie AG, Althofen, Austria

3 Institute of Energy and Climate Research (IEK-1), Forschungszentrum Jülich GmbH, Jülich, Germany

Introduction

Thermal barrier coatings (TBC) are used in the hot sections of land-based and aero gas turbine engine components to insulate the underlying metallic material from high temperatures. 7-8 wt.% YSZ is the standard ceramic material used for TBC applications due to its low thermal conductivity, phase stability up to 1200 °C, high fracture toughness, and high coefficient of thermal expansion (CTE). The gas turbine efficiency can be increased by increasing the gas inlet temperature (Ref 1, 2). However, above 1200 °C, the standard top coat TBC material, YSZ undergoes significant sintering, undesirable phase transformation and CMAS (calcium magnesium alumino silicates) degradation which limits the long durability of TBC (Ref 3-9). During

the past decade, new ceramic materials such as the pyrochlores, perovskites, and the hexaaluminates materials have been proposed for high temperature (>1200 °C) TBC applications (Ref 10). Among the new ceramic materials, pyrochlores of rare earth zirconate composition such as gadolinium zirconate (GZ) have shown the potential to replace YSZ as the top coat for high temperature applications due to their lower thermal conductivity than YSZ, CMAS attack resistance and excellent phase stability (Ref 10-14). However, GZ has a poor thermochemical compatibility with the thermally grown oxide (TGO) which results in lower thermal cyclic life of GZ single-layer TBCs compared to the YSZ single-layer TBC (Ref 15). Therefore, double-layered gadolinium zirconate/YSZ TBCs are used and it was shown that the double-layered TBCs have a higher thermal cyclic life compared to the single-layer YSZ (Ref 12, 16-18).

In TBCs, high erosion resistance of the ceramic top coat is highly desirable as it has a direct influence on the TBC performance. Recently, Nicholls et al. demonstrated that EB-PVD (electron beam physical vapor deposition) deposited 8YSZ TBCs possess better erosion resistance compared to APS (Atmospheric Plasma Spray) due to their columnar microstructure (Ref 19, 20). However, EB-PVD is a relatively expensive process with lower deposition rates than APS. Suspension plasma spray (SPS), a modification of APS process, has shown the potential to generate columnar microstructures (Ref 21, 22). A higher erosion resistance of SPS deposited YSZ-based TBCs compared to the APS deposited YSZ TBCs was reported (Ref 23). Very recently, Mahade et al. (Ref 12, 24) reported columnar microstructure in GZ/YSZ multi-layered TBCs deposited by SPS process.

In addition to the TBC deposition process, the porosity content of a TBC influences the erosion performance. It was demonstrated by Ramachandran et al. (Ref 25) that a relatively denser TBC can help in improving the erosion performance over the porous TBCs. Also, a thin denser TBC layer on top was proposed by Viswanathan et al. (Ref 26) to improve the erosion performance of the GZ-based multilayered TBCs deposited by APS process.

To the best of author's knowledge, no attempt has been made so far to evaluate the erosion resistance of SPS deposited GZ-based TBCs with columnar microstructure. In this study, single-layer 8YSZ along with GZ/YSZ double-layer TBC was deposited by SPS process. Additionally, a triple-layer TBC (GZdense/GZ/YSZ) comprising denser 30-μm-thick GZ layer on top of GZ/YSZ TBC was deposited by SPS process in order to impart a better erosion resistance. The GZ/YSZ multi-layered TBCs were evaluated for their erosion resistance at room temperature and compared with 8YSZ single-layer TBC.

Experimental Details

Specimen Preparation

Stainless steel (SS 304) substrates of 50 mm × 50 mm × 3 mm dimensions were grit-blasted using alumina particles of 220 μm grit size to create a roughness profile of 3 ± 1 μm on R_a scale. A 220-μm-thick bond coat of NiCoCrAlY (AMDRY 386-2) composition was deposited on the grit-blasted substrates using the HVAF (high velocity air fuel) process (M3 gun, UniqueCoat, Virginia, USA).The bond-coated TBCs were again grit-blasted to obtain a surface roughness profile of 5 ± 1.5 μm (R_a). The grit media were white fused alumina (Washington Mills, USA) of 220 grit size. The grit-blasting step was carried out using UniqueCoat feeder system to remove the oxides from the surface.

Suspension Properties and Process Parameters

For this study, three different ethanol-based suspensions were provided by Treibacher Industrie AG, Austria. First suspension comprised of 8YSZ with a median particle size of 500 nm and a solid load of 25 wt.%. Second suspension comprised of GZ with a median particle size of 500 nm and a solid load 25 wt.%. Third suspension was GZ with a median particle size of 1 μm and solid load content in the suspension was kept at 40 wt.%.

Axial suspension plasma spray process was employed to deposit the single-layer YSZ and GZ-based multi-layered TBCs. Three different TBC architectures were sprayed using Axial III plasma gun (Northwest Mettech Corp; Canada), as shown in Fig. 1. The first variation comprised of single-layer 8YSZ, and the second architecture comprised of GZ/YSZ double-layer TBC with GZ as the top layer and YSZ as the intermediate layer. The third variation comprised of a triple-layer TBC with GZ dense on top of GZ/YSZ TBC. Two different spray parameters were used to deposit the single-layer YSZ and GZ-based multi-layered TBCs, as shown in Table 1.

Coating Characterization

Microstructural Analysis

The as-sprayed TBCs were cold-mounted using low-viscosity epoxy resin and then sectioned using slow speed diamond cutter. The sectioned samples were again cold-mounted using high-viscosity epoxy resin. The details of polishing steps are discussed in our previous work (Ref 12). The scratch-free mirror-polished TBC samples were gold-sputtered prior to scanning electron microscopy
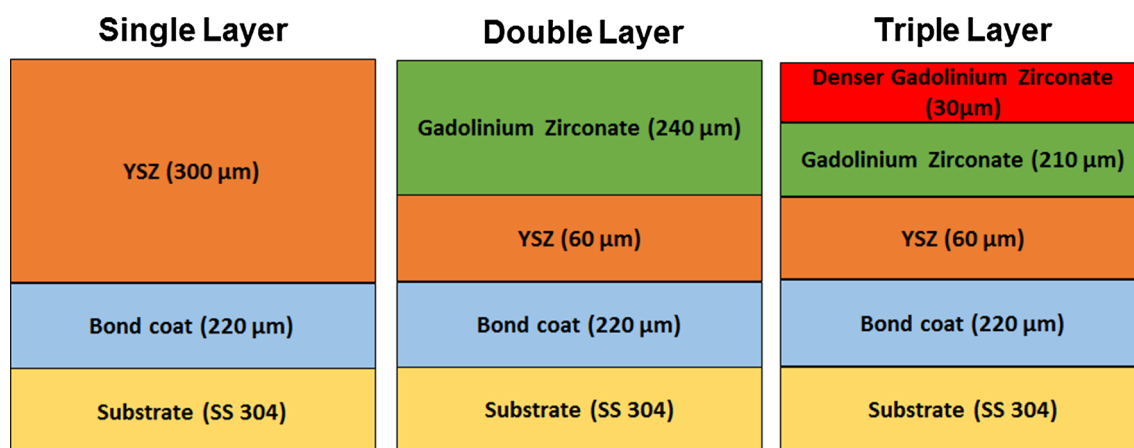
Fig. 1 Different TBC architectures deposited by SPS process

Table 1 Spray parameters used for depositing different layers of the single-, double- and triple-layer TBCs

Parameters	Columnar	Denser
Solvent	Ethanol	Ethanol
Median particle size of solute (nm)	500	1000
Solid load content in suspension (wt.%)	25	40
Standoff distance (mm)	100	70
Enthalpy (kJ)	11.2	12.5
Power (kW)	122	89

(SEM) analysis. Cross section and top surface of as-sprayed TBCs were analyzed by scanning electron microscopy (Hitachi TM 3000, Japan) in backscattered electron mode. Twenty-five different SEM micrographs at low magnification (250×) were used to measure the thickness of as-sprayed TBCS.

Porosity Measurement

Porosity measurements were made using water intrusion method and image analysis method.

Water Intrusion Method The porosity measurements were made according to ISO 18754:2013 (Ref 27). Free standing coatings of the as-sprayed TBCs were obtained by immersing the TBC in a solution of HNO_3 and HCl. The coatings were dried in an oven at 150 °C for an hour to remove the entrapped liquid. The dry weight of the free standing coatings was measured. The coatings were set in a water beaker, and the setup was then placed in a vacuum chamber. The setup was vacuumed several times in order to remove the entrapped air from the pores of the free standing coating and allow water to infiltrate the pores. The wet weight of the coatings was measured after removing them from the water beaker. The difference in weight is the weight of water infiltrated in the coating, and the porosity content of the coating was calculated. This method, however, does not take into account the closed porosity of the coating as water cannot infiltrate the closed pores. Therefore, an additional method which can estimate both open and closed porosity of a coating is highly desirable.

Image Analysis This method can estimate both open and closed porosities in a coating. Twenty-five different SEM micrographs at 500× magnification were considered for the porosity measurement by image analysis using the Image J software (Ref 28). The porosity mean values along with the standard deviation were reported.

Micro-hardness Measurement

Hardness measurements on Vickers scale were made using an HMV-2 series micro-hardness tester (SHIMADZU Corp., Japan). A square pyramidal-shaped diamond indenter was used. Micro-hardness measurements were made on the cross section of the TBC specimen at two different loads (0.3 and 0.5 N). Fifteen different hardness measurements were made at each load, and their mean hardness value along with the standard deviations is reported. At higher loads (0.5 N), cracks at the indent vertices were observed due to the brittle nature of ceramics.

Phase Analysis

The phase composition of the top surface of as-sprayed TBCs was analyzed using Seifert TT 3003 x-ray diffractometer. Cu Kα of 1.54 Å wavelength in the two theta range of 20°-70° was used.

Erosion Test

Erosion test at room temperature was performed at Forschungszentrum Jülich, Germany (IEK-1) according to GE specification no. E50TF121. Aluminum oxide particles of 240 # grit size were used as the eroding media. The test specimen were held at an angle of $20° \pm 2°$ to the axis of blast nozzle, and the thickness loss at the end of 90 s was measured using a 0.250-inch-diameter ball tip micrometer. Erosivity number, (seconds/mils) which is the ratio of time to spray and thickness loss, of the single-, double- and triple-layer TBCs was calculated.

Results and Discussion

Microstructure Analysis

The as-sprayed TBC microstructures were analyzed by SEM. In the cross-sectional view, YSZ single-layer TBC showed a columnar microstructure, as seen in Fig. 2(a). Thickness of YSZ layer was found to be approximately 300 ± 10 µm. The top view surface morphology showed microstructure resembling a cauliflower, as seen in Fig. 2(b).

The double-layer GZ/YSZ TBC also showed a columnar microstructure, as seen in Fig. 3(a). Thickness of the intermediate YSZ layer was found to be approximately 60 µm, whereas the top GZ layer had a thickness of approximately 240 µm. The total thickness of ceramic layer was approximately 300 ± 15 µm. The top surface morphology of the double-layer TBC showed a cauliflower look alike microstructure, as seen in Fig. 3(b).

In the case of triple-layer TBC, a denser GZ layer of approximately 30 µm thickness could be seen on top of the relatively porous GZ layer and YSZ layer, as shown in Fig. 4(a). The cross-sectional SEM microstructure is also columnar with an overall coating thickness of approximately 300 ± 15 µm. The top surface morphology of triple-layer TBC resembles cauliflower microstructure, and it looks relatively denser compared to the top surface morphology of double-layer TBC, as seen in Fig. 4(b). A higher magnification SEM micrograph of triple-layer TBC shows a clearly visible denser GZ layer on top of the relatively porous GZ layer, as seen in Fig. 4(c).

Porosity Measurement

Water Intrusion Method

In this method, the double- and triple-layer TBCs were treated as single unit and their overall porosity content was calculated. All the pores in the coating which are accessible by water can be measured by this method (open pores). It was observed that the single-layer YSZ TBC had the highest porosity content of approximately 21%, whereas the double-layer TBC had an overall porosity content of approximately 18% as shown in Fig. 5. Triple-layer TBC had the lowest porosity content of approximately 17% and the reason could be due to the presence of the denser GZ layer on top.

Image Analysis

Porosity values of the as-sprayed TBCs obtained by this method differ from those estimated by water intrusion method, as seen in Fig. 5. However, the ranking of the porosity content of single-, double- and triple-layer TBCs was the same using both the methods. A possible explanation for the difference in porosity values estimated by this method could be due to the fact that this method can measure both open and closed pores of a coating. However, at lower magnification (500×), the fine-scale porosity in the coating is difficult to be taken into account using this method.

Micro-hardness Test

The hardness values of YSZ and GZ at 0.3 N load were approximately 560 ± 20 $Hv_{0.3}$ and 605 ± 30 $Hv_{0.3}$,

Fig. 2 SEM micrographs of the single-layer 8YSZ TBC (a) cross section (b) top surface morphology
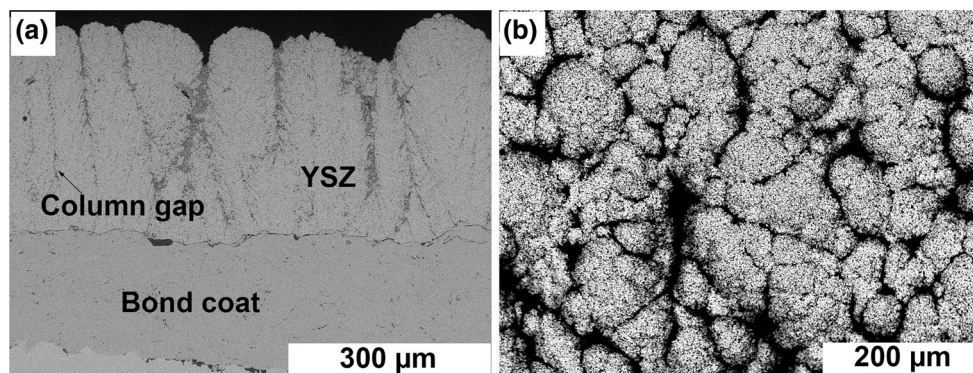
Fig. 3 SEM micrographs of the double-layer GZ/YSZ TBC (a) cross section (b) top surface morphology
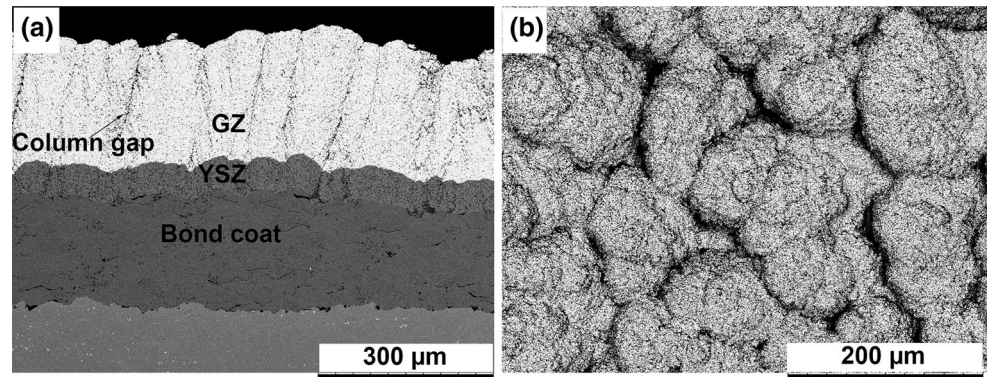

Fig. 4 SEM micrographs of the triple-layer TBC (a) cross section (b) top surface morphology (c) higher magnification cross-sectional micrograph
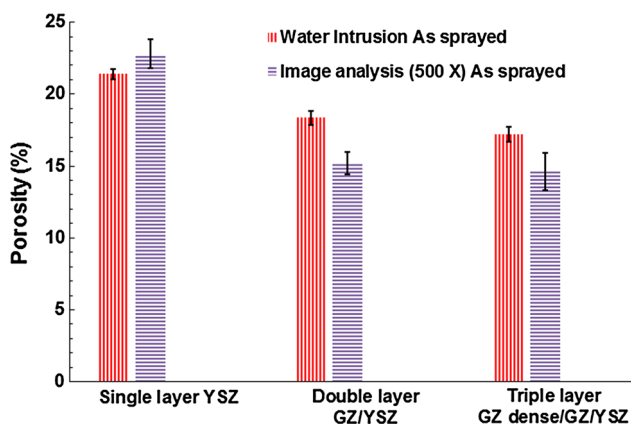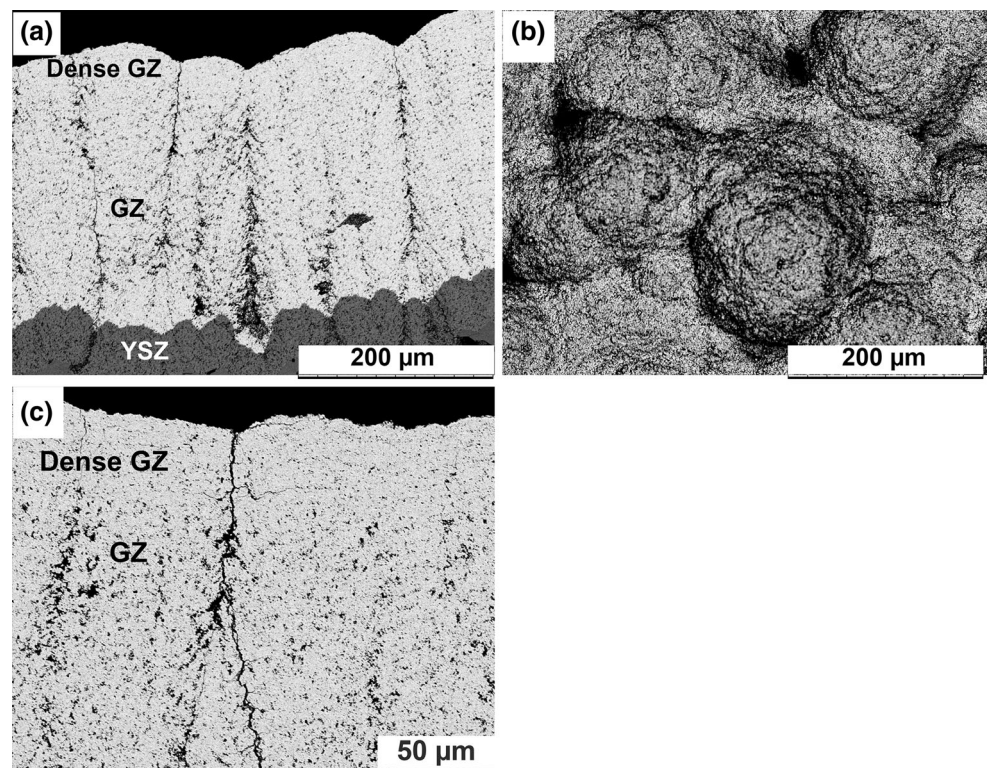

Fig. 5 Porosity content of the as-sprayed TBCs estimated by water intrusion method and image analysis method

respectively. GZ showed a slightly higher hardness compared to YSZ. At higher load (0.5 N), the micro-hardness values of GZ and YSZ showed a similar ranking where GZ had a slightly higher hardness than YSZ (646 ± 35 and 622 ± 25, respectively).

Phase Analysis

The peaks obtained by XRD analysis were identified using JCPDS standard and labeled accordingly, as shown in Fig. 6. 8YSZ single-layer TBC showed a tetragonal prime zirconia phase, which is a metastable phase of tetragonal zirconia with yttria as the stabilizer. The metastable phase is highly desirable as it remains stable in the temperature range of 25-1200 °C without undergoing phase transformation which

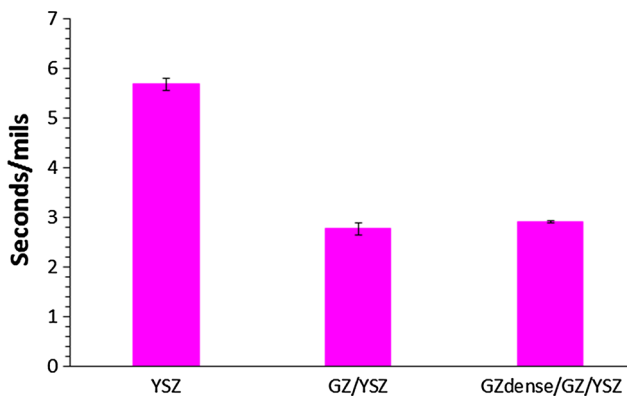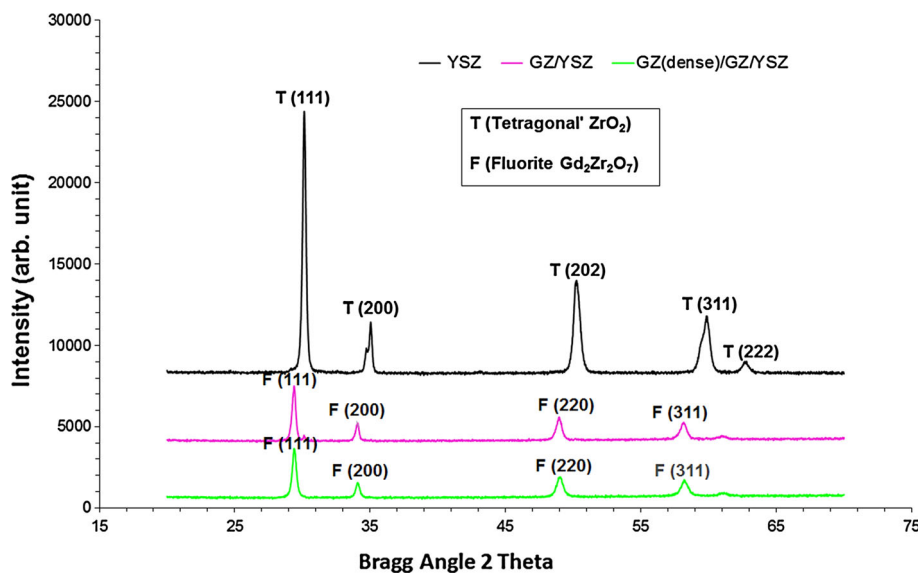**Fig. 6** XRD analysis of the as-sprayed TBCs

Fig. 7 Erosion resistance of the as-sprayed TBCs

results in improvement in the thermal cyclic life of the TBC. In the case of GZ-based double- and triple-layered TBCs, cubic defect fluorite phase was found. The defect fluorite phase transforms to cubic pyrochlore structure when exposed to higher temperature. Defect fluorite is a disordered variation of pyrochlore structure where the cations and oxygen vacancies occupy random positions in the cubic crystal structure. Change in suspension parameters for depositing the denser GZ layer in the case of triple-layer TBC which comprised of higher solid load content (40 wt.%) and higher median particle size (1 μm) of GZ did not alter the stoichiometry.

Erosion Test

Erosivity numbers of the single-, double- and triple-layer TBCs are plotted in Fig. 7. A higher erosivity number of a TBC indicates a higher erosion resistance. Among the as-sprayed TBCs, double-layer GZ/YSZ TBC had the lowest

erosion resistance. Triple-layer GZ dense/GZ/YSZ TBC showed a slight improvement in erosion resistance than double-layer TBC due to the presence of relatively denser GZ on top. A similar observation on improvement in erosion resistance of relatively denser TBC than a porous TBC of same composition was reported (Ref [25]). The single-layer 8YSZ TBC showed a higher erosion resistance (approximately two times better) than the GZ-based multi-layered TBCs. In this work, YSZ showed a slightly higher porosity and lower hardness than the GZ-based TBCs which would favor a better erosion resistance of GZ-based TBCs than YSZ single-layer TBC. However, the erosion resistance of GZ-based TBCs was poor compared to YSZ and the reason could be due to the lower fracture toughness of GZ (1.02 ± 0.11 MPa m$^{1/2}$) than YSZ (~ 2 MPa m$^{1/2}$) (Ref [17]). A higher fracture toughness allows the ceramic material to absorb more energy from the alumina particles before being eroded. A similar observation on poor erosion resistance of APS deposited rare earth zirconate (lanthanum zirconate) TBCs compared to YSZ was reported (Ref [20], [25]).

Eroded TBCs were analyzed by SEM. Single-layer YSZ showed a lower coating thickness loss compared to multi-layered TBCs after the erosion test at room temperature, as seen in Fig. 8(a). Also, the delamination within YSZ and close to the point of impact with eroding media was observed at a higher magnification, as shown in Fig. 8(b). Similar delamination cracks within YSZ were reported for EB-PVD processed YSZ-based TBC after the erosion test (Ref [29]). In the case of eroded GZ/YSZ double-layer TBC, thickness loss of GZ layer was higher than single-layer YSZ TBC, as seen in Fig. 9(a). However, TBC delamination was not observed in the eroded GZ/YSZ TBC and the cross-sectional SEM micrograph looked similar to the as-

Fig. 8 SEM micrographs of the eroded single-layer YSZ (a) low magnification (b) higher magnification
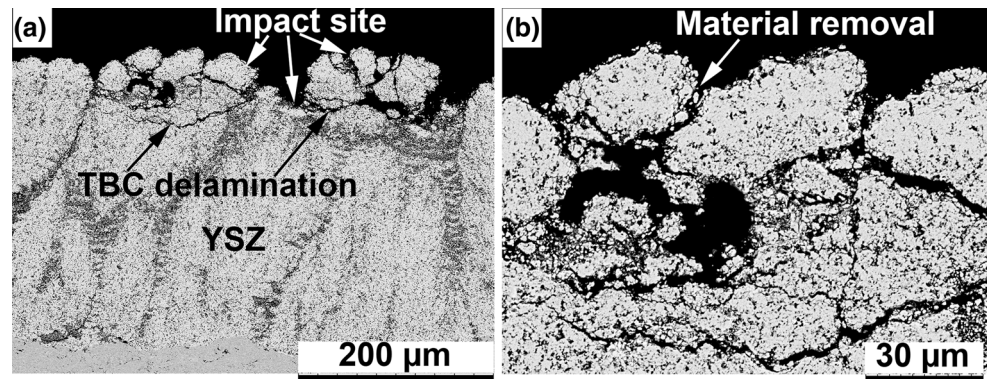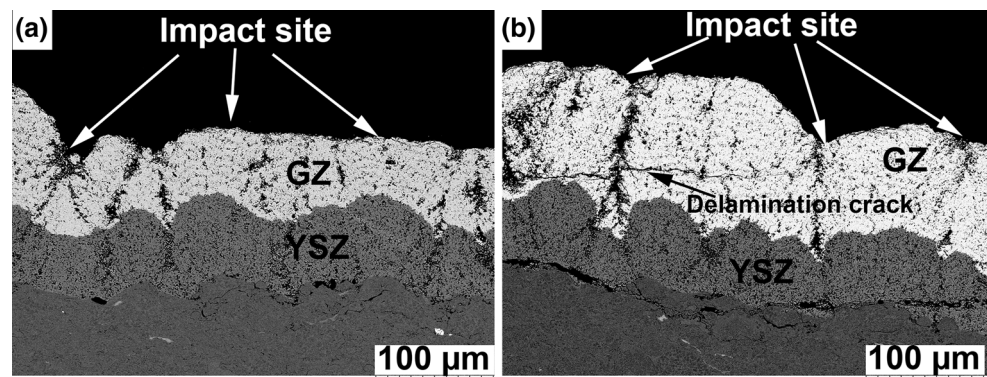

Fig. 9 SEM micrographs of the eroded GZ-based multi-layered TBCs (a) GZ/YSZ double-layer TBC (b) GZdense/GZ/YSZ triple-layer TBC

sprayed microstructure, but with a reduced thickness of GZ layer, as seen in Fig. 9(a). In the case of eroded triple-layer TBC, thickness reduction was relatively lower compared to the double-layer TBC, as seen in Fig. 9(b). It seems that a higher amount of erodent is required to erode a dense layer than a relatively porous layer. Also, a horizontal delamination crack was observed in the eroded triple-layer TBC close to the GZ/YSZ interface.

Conclusion

In this work, standard 8YSZ single-layer TBC along with GZ/YSZ multi-layered TBCs were deposited by suspension plasma spray process and their erosion resistance at room temperature was compared. It was shown that:-

- Single-layer 8YSZ had a higher erosion resistance than GZ/YSZ multi-layered TBCs despite of its higher porosity content and slightly lower hardness among the as-sprayed TBCs.
- A denser GZ top layer in the case of triple-layer TBC helped in slightly improving the erosion resistance compared to the GZ/YSZ double-layer TBC.

References

1. R.A. Miller, Thermal Barrier Coatings for Aircraft Engines: History and Directions, *J. Therm. Spray Technol.*, 1997, **6**(1), p 35-42
2. D. Stöver and C. Funke, Directions of the Development of Thermal Barrier Coatings in Energy Applications, *J. Mater. Process. Technol.*, 1999, **92–93**, p 195-202
3. J.M. Drexler, C.-H. Chen, A.D. Gledhill, K. Shinoda, S. Sampath, and N.P. Padture, Plasma Sprayed Gadolinium Zirconate Thermal Barrier Coatings That are Resistant to Damage by Molten Ca–Mg–Al–Silicate Glass, *Surf. Coat. Technol.*, 2012, **206**(19–20), p 3911-3916
4. A.D. Gledhill, K.M. Reddy, J.M. Drexler, K. Shinoda, S. Sampath, and N.P. Padture, Mitigation of Damage from Molten Fly Ash to Air-Plasma-Sprayed Thermal Barrier Coatings, *Mater. Sci. Eng. A*, 2011, **528**(24), p 7214-7221
5. L. Li, N. Hitchman, and J. Knapp, Failure of Thermal Barrier Coatings Subjected to CMAS Attack, *J. Therm. Spray Technol.*, 2009, **19**(1–2), p 148-155
6. A. Aygun, A.L. Vasiliev, N.P. Padture, and X. Ma, Novel Thermal Barrier Coatings that are Resistant to High-Temperature Attack by Glassy Deposits, *Acta Mater.*, 2007, **55**(20), p 6734-6745
7. A. Cipitria, I.O. Golosnoy, and T.W. Clyne, A Sintering Model for Plasma-Sprayed Zirconia TBCs. Part I: Free-Standing Coatings, *Acta Mater.*, 2009, **57**(4), p 980-992
8. S. Krämer, J. Yang, and C.G. Levi, Infiltration-Inhibiting Reaction of Gadolinium Zirconate Thermal Barrier Coatings with CMAS Melts, *J. Am. Ceram. Soc.*, 2008, **91**(2), p 576-583

9. S. Krämer, J. Yang, C.G. Levi, and C.A. Johnson, Thermochemical Interaction of Thermal Barrier Coatings with Molten CaO–MgO–Al$_2$O$_3$–SiO$_2$ (CMAS) Deposits, *J. Am. Ceram. Soc.*, 2006, **89**(10), p 3167-3175

10. R. Vaßen, M.O. Jarligo, T. Steinke, D.E. Mack, and D. Stöver, Overview on Advanced Thermal Barrier Coatings, *Surf. Coat. Technol.*, 2010, **205**(4), p 938-942

11. N.P. Padture, M. Gell, and E.H. Jordan, Thermal Barrier Coatings for Gas-Turbine Engine Applications, *Science*, 2002, **296**(5566), p 280-284

12. S. Mahade, N. Curry, S. Björklund, N. Markocsan, and P. Nylén, Thermal Conductivity and Thermal Cyclic Fatigue of Multilayered Gd2Zr2O7/YSZ Thermal Barrier Coatings Processed by Suspension Plasma Spray, *Surf. Coat. Technol.*, 2015, **283**, p 329-336

13. G. Moskal, L. Swadźba, M. Hetmańczyk, B. Witala, B. Mendala, J. Mendala, and P. Sosnowy, Characterization of Microstructure and Thermal Properties of Gd2Zr2O7-Type Thermal Barrier Coating, *J. Eur. Ceram. Soc.*, 2012, **32**(9), p 2025-2034

14. G. Mauer, M.O. Jarligo, D.E. Mack, and R. Vaßen, Plasma-Sprayed Thermal Barrier Coatings: New Materials, Processing Issues, and Solutions, *J. Therm. Spray Technol.*, 2013, **22**, p 646-658

15. R.M. Leckie, S. Krämer, M. Rühle, and C.G. Levi, Thermochemical Compatibility Between Alumina and ZrO$_2$–GdO$_{3/2}$ Thermal Barrier Coatings, *Acta Mater.*, 2005, **53**(11), p 3281-3292

16. E. Bakan, D.E. Mack, G. Mauer, and R. Vaßen, Gadolinium Zirconate/YSZ Thermal Barrier Coatings: Plasma Spraying, Microstructure, and Thermal Cycling Behavior, *J. Am. Ceram. Soc.*, 2014, **97**(12), p 4045-4051

17. X. Zhong, H. Zhao, C. Liu, L. Wang, F. Shao, X. Zhou, S. Tao, and C. Ding, Improvement in Thermal Shock Resistance of Gadolinium Zirconate Coating by Addition of Nanostructured Yttria Partially-Stabilized Zirconia, *Ceram. Int.*, 2015, **41**(6), p 7318-7324

18. K.S. Lee, D.H. Lee, and T.W. Kim, Microstructure Controls in Gadolinium Zirconate/YSZ Double Layers and Their Properties, *J. Ceram. Soc. Jpn.*, 2014, **122**(1428), p 668-673

19. J.R. Nicholls, M.J. Deakin, and D.S. Rickerby, A Comparison Between the Erosion Behaviour of Thermal Spray and Electron Beam Physical Vapour Deposition Thermal Barrier Coatings, *Wear*, 1999, **233–235**, p 352-361

20. R.G. Wellman and J.R. Nicholls, A Review of the Erosion of Thermal Barrier Coatings, *J. Phys. Appl. Phys.*, 2007, **40**(16), p R293

21. P. Sokołowski, S. Kozerski, L. Pawłowski, and A. Ambroziak, The key Process Parameters Influencing Formation of Columnar Microstructure in Suspension Plasma Sprayed Zirconia Coatings, *Surf. Coat. Technol.*, 2014, **260**, p 97-106

22. N. Curry, Z. Tang, N. Markocsan, and P. Nylén, Influence of Bond Coat Surface Roughness on the Structure of Axial Suspension Plasma Spray Thermal Barrier Coatings—Thermal and Lifetime Performance, *Surf. Coat. Technol.*, 2015, **268**, p 15-23

23. N. Curry, K. VanEvery, T. Snyder, and N. Markocsan, Thermal Conductivity Analysis and Lifetime Testing of Suspension Plasma-Sprayed Thermal Barrier, *Coatings*, 2014, **4**(3), p 630-650

24. S. Mahade, R. Li, N. Curry, S. Björklund, N. Markocsan, and P. Nylén, Isothermal Oxidation Behavior of Gd2Zr2O7/YSZ Multilayered Thermal Barrier Coatings, *Int. J. Appl. Ceram. Technol.*, 2016, **13**(3), p 443-450

25. C.S. Ramachandran, V. Balasubramanian, and P.V. Ananthapadmanabhan, Erosion of Atmospheric Plasma Sprayed Rare Earth Oxide Coatings Under Air Suspended Corundum Particles, *Ceram. Int.*, 2013, **39**(1), p 649-672

26. V. Viswanathan, G. Dwivedi, and S. Sampath, Multilayer, Multimaterial Thermal Barrier Coating Systems: Design, Synthesis, and Performance Assessment, *J. Am. Ceram. Soc.*, 2015, **98**(6), p 1769-1777

27. "ISO 18754:2013—Fine Ceramics (Advanced Ceramics, Advanced Technical Ceramics)—Determination of Density and Apparent Porosity," *ISO*. [Online]. http://www.iso.org/iso/iso_catalogue/catalogue_tc/catalogue_detail.htm?csnumber=55448

28. "ImageJ," *Softonic*. [Online]. http://imagej.en.softonic.com/

29. N.A. Fleck and T. Zisis, The Erosion of EB-PVD Thermal Barrier Coatings: The Competition Between Mechanisms, *Wear*, 2010, **268**(11–12), p 1214-1224